5

Scanning Multi-sensor System for Measurement of Roundness

5.1 Introduction

Roundness is one of the most fundamental geometries of precision workpieces. Most of the round-shaped precision workpieces are manufactured by a turning process, in which a spindle is employed to rotate the workpiece. The out-of-roundness of the workpiece is basically determined by the error motion of the spindle. Measurement of the workpiece roundness error and the spindle error is an essential task for assurance of the manufacturing accuracy.

The scanning sensor method [1, 2] is the most widely used method for the measuring the roundness of a workpiece. In this method, a displacement sensor or a slope sensor, which is mounted on a rotary stage, is moved to scan the workpiece surface. The rotational scanning motion of the stage must be good enough so that it can be used as the measurement reference. To nanometrically roundness, however, the required measurement accuracy of the workpiece roundness must be at the same level as that of the scanning motion of the stage. Similar cases can be found in the on-machine measurement where the machine tool spindle is used. In such cases, it is essential to separate the workpiece roundness error from the spindle error [3, 4]. The error separation is also necessary in spindle error measurement, in which a ball or a cylinder is used as the measurement reference.

To perform the error separation, it is necessary to establish simultaneous equations involving the workpiece roundness error and the spindle error. There are two kinds of error separation methods based on how the equations are established [5]. One is known as the multi-step technique [6–8], and the other is the multi-sensor technique [9–13]. The multi-step methods including the reversal method establish the equations by making multiple measurements with one sensor. On the other hand, the multi-sensor methods establish the equations by using multiple sensors to make one measurement. Compared with multi-step methods, multi-sensor methods are more suitable for on-machine measurements because the repeatability of the spindle error is not necessary.

Roundness measurement involves three parameters; roundness error of the workpiece, and the *X*-directional component and *Y*-directional component of the spindle error. The three-displacement sensor method [14], which employs three displacement sensors, can realize the error separation to get the accurate workpiece roundness. In this chapter, a new three-sensor method of using three 2D slope sensors, called the three-slope sensor method, is presented to measure not only workpiece roundness but also multi-degree-of-freedom spindle error components.

However, some high-frequency components of roundness error cannot be accurately measured with the three-sensor method due to the problem of harmonic suppression. This problem cannot be completely solved by merely increasing the number of sensors [11, 14]. A new multi-sensor method, called the mixed method, is thus presented in the second part of this chapter to overcome this drawback of the three-sensor method.

5.2 Three-slope Sensor Method

Figure 5.1 shows the principle of the roundness measurement by using one displacement sensor. A displacement sensor, which is fixed spatially, is used to scan a round workpiece while the workpiece is rotating. Let *P* be a representative point of the workpiece, and the roundness error be described by the function $r(\theta)$, which is the deviation from the circle with an average radius of R_r. θ is the angle between the point *P* and the sensor. Let α be the angle between the sensor and the *Y*-axis. If no rotational error of the spindle (spindle error) exists, as shown in Figure 5.1, the roundness error $r(\theta)$ can be obtained correctly from the sensor output $m(\theta)$ as follows:

$$m(\theta) = r(\theta). \tag{5.1}$$

However, if the spindle error exists, as shown in Figure 5.2, the sensor output $m(\theta)$ becomes,

$$m(\theta) = r(\theta) + \Delta m(\theta), \tag{5.2}$$

where

$$\Delta m(\theta) = e_X(\theta)\sin\alpha + e_Y(\theta)\cos\alpha. \tag{5.3}$$

Here, $e_X(\theta)$ and $e_Y(\theta)$ are the *X*-directional and the *Y*-directional components of the spindle error.

Figure 5.2 shows the principle of the three-displacement sensor method using three displacement sensors schematically. The three displacement sensors are fixed around a cylindrical workpiece. The workpiece is scanned by the sensors while the workpiece is rotating. If the displacement outputs of the sensors are denoted by $m_1(\theta)$, $m_2(\theta)$ and $m_3(\theta)$, respectively, the outputs can be expressed as:

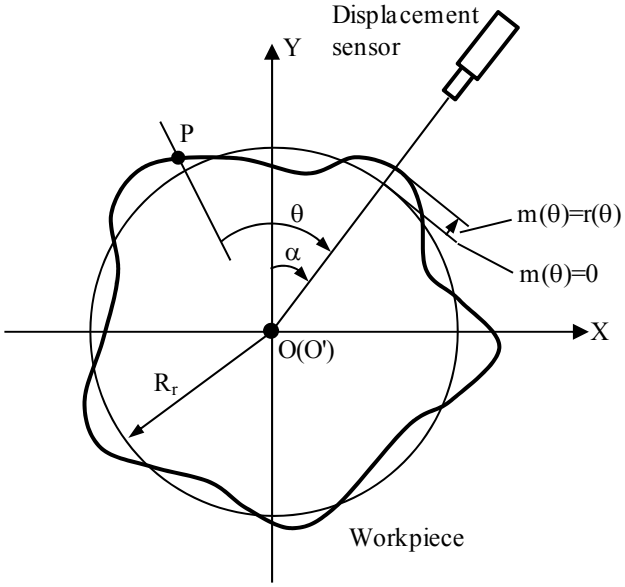

(a) Without spindle error

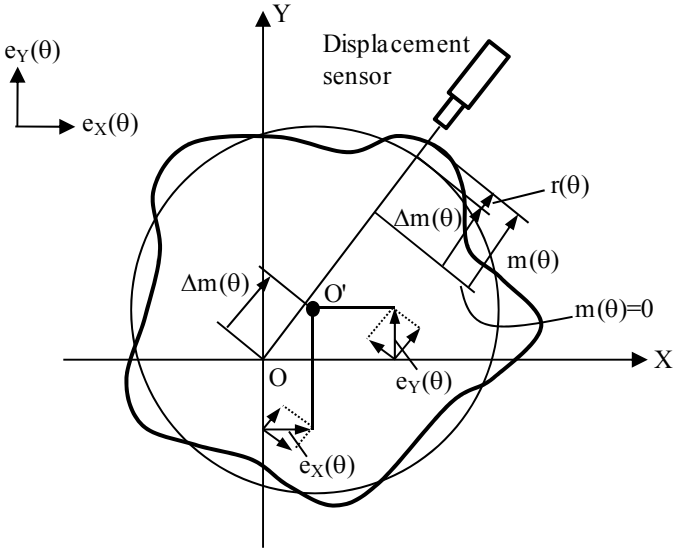

(b) With spindle error

Figure 5.1. Roundness measurement by using a displacement sensor

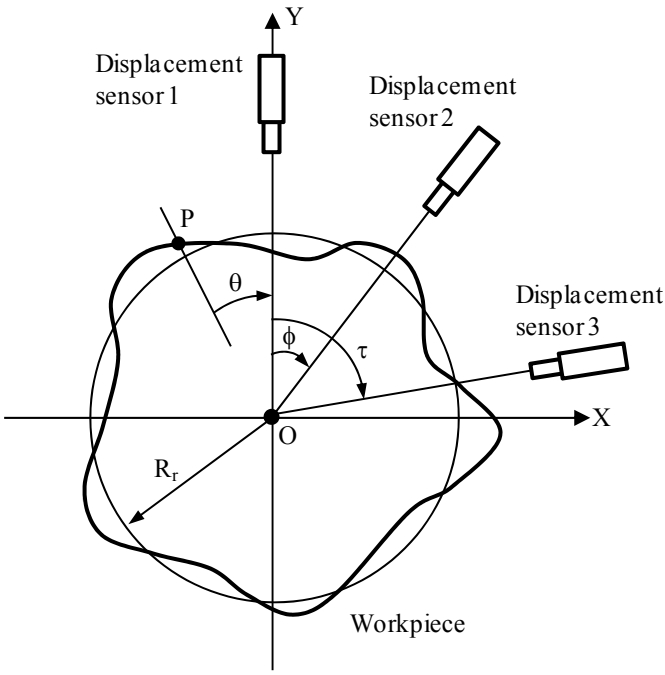

Figure 5.2. The three-displacement sensor method for roundness measurement

$$m_1(\theta) = r(\theta) + e_Y(\theta), \tag{5.4}$$

$$m_2(\theta) = r(\theta + \phi) + e_X(\theta)\sin\phi + e_Y(\theta)\cos\phi, \tag{5.5}$$

$$m_3(\theta) = r(\theta + \tau) + e_X(\theta)\sin\tau + e_Y(\theta)\cos\tau. \tag{5.6}$$

The differential output $m_{3D}(\theta)$ of the three-displacement sensor method, in which the spindle error is canceled, can be denoted as

$$m_{3D}(\theta) = r(\theta) + a_1 r(\theta + \phi) + a_2 r(\theta + \tau), \tag{5.7}$$

where

$$a_1 = -\frac{\sin\tau}{\sin(\tau - \phi)},\ a_2 = \frac{\sin\phi}{\sin(\tau - \phi)}. \tag{5.8}$$

In Equation 5.7, $r(\theta)$ can be treated as the input and $m_{3D}(\theta)$ as the output. According to the theory of digital filters [15], the relation between the input $r(\theta)$ and the output $m_{3D}(\theta)$ can be defined by the following transfer function of the three-displacement sensor method:

$$H_{3D}(n) = \frac{M_{3D}(n)}{R(n)} = 1 + a_1 e^{-jn\phi} + a_2 e^{-jn\tau}, \tag{5.9}$$

where n is the spatial frequency (the number of undulations per revolution), and $M_{3D}(n)$ and $R(n)$ are the Fourier transforms of $m_{3D}(\theta)$ and $r(\theta)$, respectively. $R(n)$ can be obtained from $M_{3D}(n)$ and $H_{3D}(n)$. $r(\theta)$ can be evaluated by IFFT of $R(n)$.

The amplitude of the transfer function $H_{3D}(n)$ represents the complex harmonic sensitivity of the three-displacement sensor method. The amplitude (harmonic sensitivity) and the phase angle of $H_{3D}(n)$ are expressed as follows:

$$\left|H_{3D}(n)\right| = \sqrt{1 + a_1^2 + a_2^2 + 2(a_1 \cos n\phi + a_2 \cos n\tau + a_1 a_2 \cos n(\tau - \phi))}, \tag{5.10}$$

$$\arg\left[H_{3D}(n)\right] = \tan^{-1}\left(-\frac{a_1 \sin n\phi + a_2 \sin n\tau}{1 + a_1 \cos n\phi + a_2 \cos n\tau}\right). \tag{5.11}$$

The transfer function $H_{3D}(\omega)$ is shown in Figure 5.3. As can be seen in the figure, the amplitude at some frequencies in the transfer function of the three-displacement sensor method approaches zero. This prevents the three-displacement sensor method from measuring the corresponding frequency components correctly.

As shown in Figure 5.4, we can also use one slope sensor to perform roundness measurement.

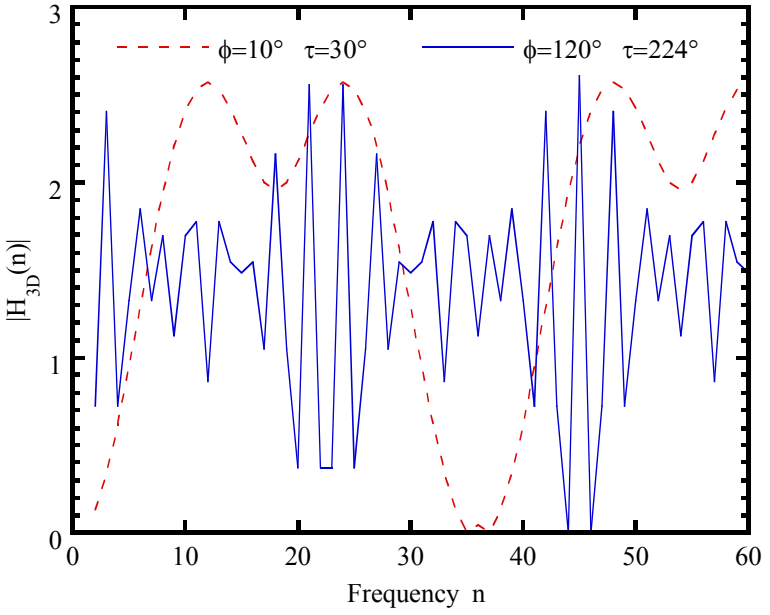

Figure 5.3. The harmonic sensitivity of the three-displacement sensor method for roundness measurement

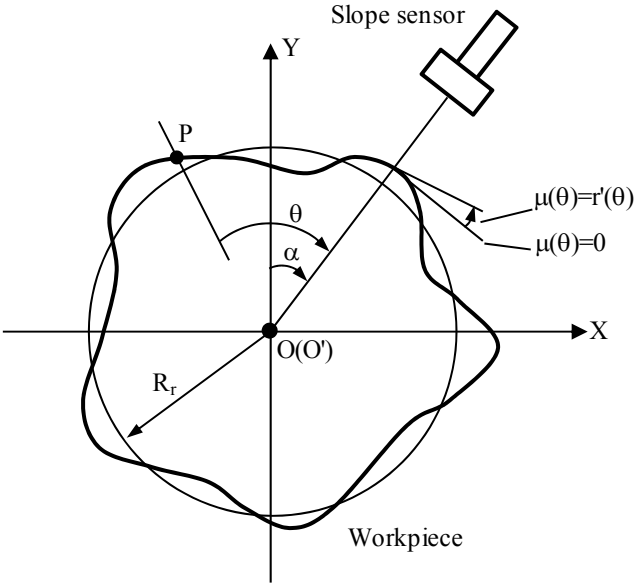

(a) Without spindle error

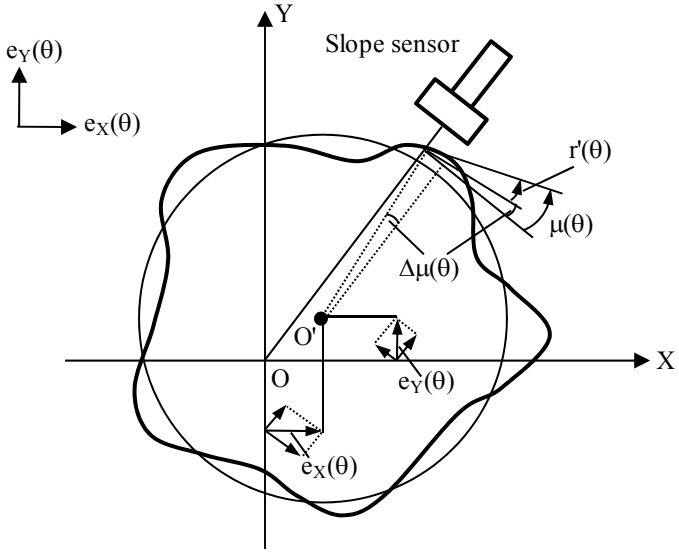

(b) With spindle error

Figure 5.4. Roundness measurement by using a slope sensor

Let the local slope of the surface be described by the function $r'(\theta)$. If no spindle error exists (Figure 5.4 (a)), the local slope $r'(\theta)$ can be measured correctly from the output of the slope sensor as [16]:

$$\mu(\theta) = r'(\theta)\,, \tag{5.12}$$

$$r'(\theta) = \frac{dr(\theta)}{d(R_r\theta)}\,. \tag{5.13}$$

where R_r is the average radius of the workpiece.

The roundness error can then be obtained by integrating $r'(\theta)$. However, if there exists a spindle error as shown in Figure 5.4 (b), because of the shift of the measuring point on the circumference of the workpiece, the spindle error will generate an angle change $\Delta\mu(\theta)$ in the sensor output as follows:

$$\mu(\theta) = r'(\theta) + \Delta\mu(\theta)\,, \tag{5.14}$$

where

$$\Delta\mu(\theta) = \frac{e_X(\theta)\cos\alpha - e_Y(\theta)\sin\alpha}{R_r}\,. \tag{5.15}$$

Figure 5.5 shows the principle of the three-slope sensor method using three-slope sensors schematically. The three-slope sensors are fixed around a cylindrical workpiece, and scan the workpiece while it is rotating. If the slope outputs of the sensors are denoted by $\mu_1(\theta)$, $\mu_2(\theta)$ and $\mu_3(\theta)$, respectively, the outputs can be expressed as:

$$\mu_1(\theta) = r'(\theta) + \frac{e_X(\theta)}{R_r}\,, \tag{5.16}$$

$$\mu_2(\theta) = r'(\theta+\phi) + \frac{e_X(\theta)}{R_r}\cos\phi - \frac{e_Y(\theta)}{R_r}\sin\phi\,, \tag{5.17}$$

$$\mu_3(\theta) = r'(\theta+\tau) + \frac{e_X(\theta)}{R_r}\cos\tau - \frac{e_Y(\theta)}{R_r}\sin\tau\,. \tag{5.18}$$

The differential output $m_{3S}(\theta)$ of the three-slope sensor method can be denoted as

$$m_{3S}(\theta) = r(\theta) + a_1 r(\theta+\phi) + a_2 r(\theta+\tau)\,, \tag{5.19}$$

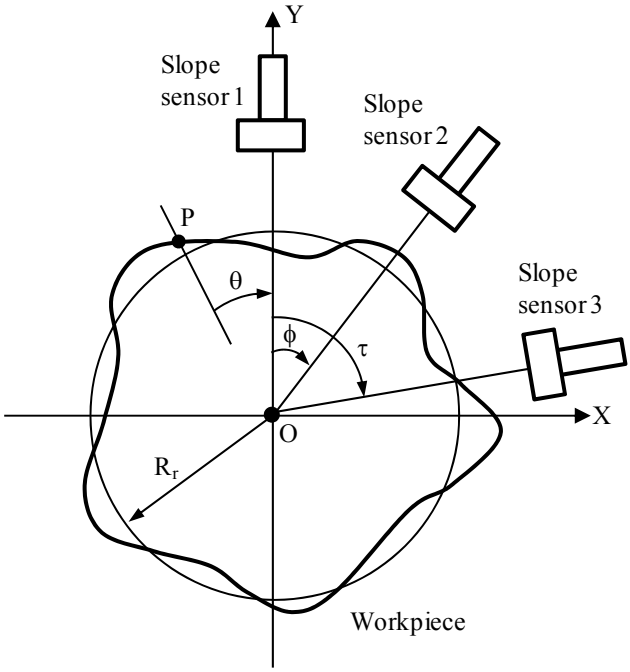

Figure 5.5. The three-slope sensor method for roundness measurement

where

$$a_1 = -\frac{\sin\tau}{\sin(\tau-\phi)},\ a_2 = \frac{\sin\phi}{\sin(\tau-\phi)}. \tag{5.20}$$

Consequently, the spindle error is canceled.

The transfer function $H_{3S}(n)$ of the three-slope sensor method can be expressed as follows:

$$H_{3S}(n) = \frac{M_{3S}(n)}{R(n)} = jn(1 + a_1 e^{-jn\phi} + a_2 e^{-jn\tau}), \tag{5.21}$$

where n is the spatial frequency (the number of undulations per revolution), and $M_{3S}(n)$ and $R(n)$ are the Fourier transforms of $m_{3S}(\theta)$ and $r(\theta)$, respectively. $R(n)$ can be obtained from $M_{3D}(n)$ and $H_{3S}(n)$. $r(\theta)$ can be evaluated by IFFT of $R(n)$. The amplitude (harmonic sensitivity) and the phase angle of $H_{3S}(n)$ are expressed as follows:

$$\left|H_{3S}(n)\right| = n\sqrt{1 + a_1^2 + a_2^2 + 2(a_1\cos n\phi + a_2\cos n\tau + a_1 a_2\cos n(\tau-\phi))}, \tag{5.22}$$

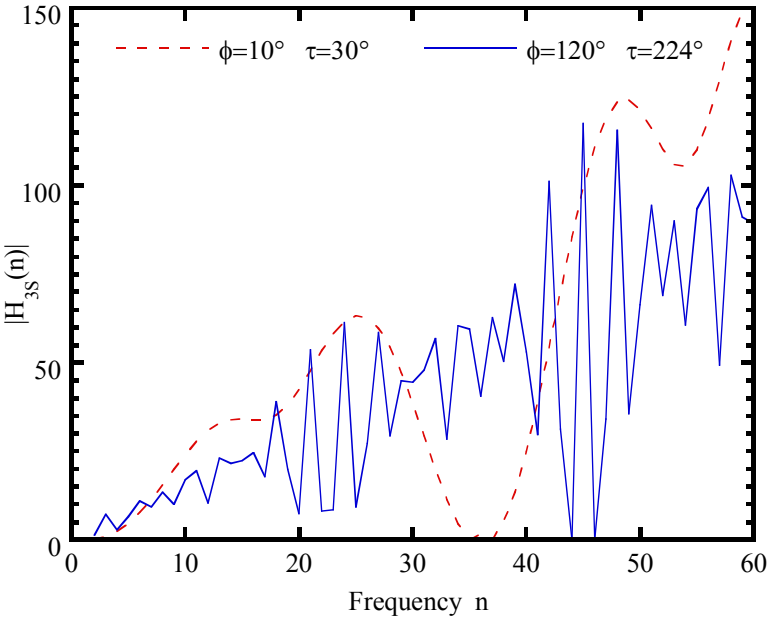

Figure 5.6. The harmonic sensitivity of the three-slope probe method for roundness measurement

$$\arg\left[H_{3S}(n)\right] = \tan^{-1}\left(\frac{1 + a_1 \cos n\phi + a_2 \cos n\tau}{a_1 \sin n\phi + a_2 \sin n\tau}\right). \tag{5.23}$$

The amplitude of the transfer function $H_{3S}(n)$ is shown in Figure 5.6. Similar to the three-displacement sensor method, the amplitude at some frequencies in the transfer function of the three-slope sensor method approaches zero. The frequencies at which the amplitude is zero are the same as those of the three-displacement sensor method with the same sensor arrangement.

The three-slope sensor method can also be used for measurement of the surface slope along the *Z*-direction and the spindle tilt error motions by using two-dimensional slope sensors. Figure 5.8 shows the schematic of the measurement principle where $r(\theta, z)$ is the surface profile of the cylindrical workpiece. Each sensor detects the two-dimensional local slopes of a point on the workpiece surface. The local slope component along the circumference direction $r'_r(\theta, z)$ is the same as that shown in Equation 5.13 and can be separated from the spindle radial error component $e_r(\theta, z)$ by using the radial output components of the slope sensors as shown in Equations 5.16–5.20. On the other hand, the local slope component along the *Z*-direction $r'_Z(\theta, z)$ is defined as:

$$r'_z(\theta) = \frac{dr(\theta, z)}{dz}. \tag{5.24}$$

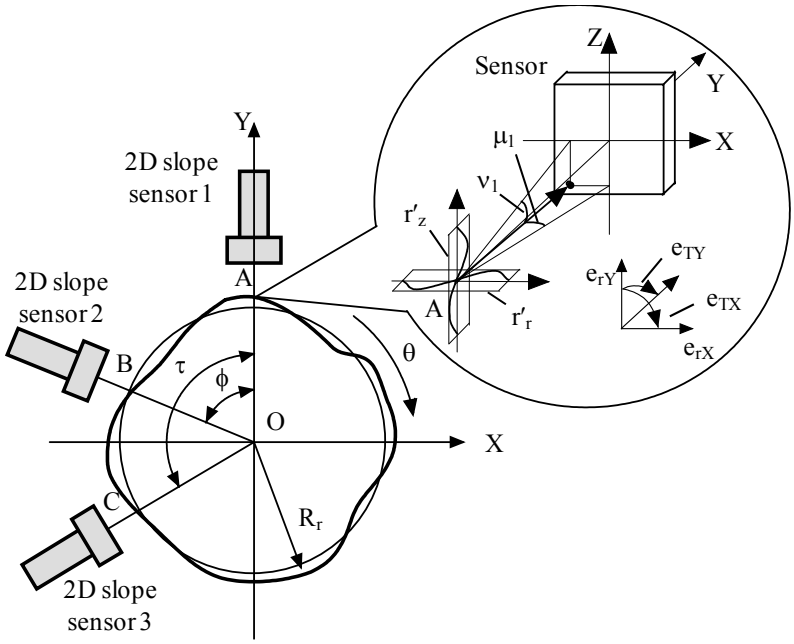

Figure 5.7. The three-slope sensor method with two-dimensional slope sensors

The $r'_Z(\theta, z)$ and the tilt error motion $e_T(\theta, z)$ can be similarly separated from each other by using the angular output components of the slope sensor shown below:

$$\nu_1(\theta) = r_z'(\theta) - e_{TY}(\theta), \tag{5.25}$$

$$\nu_2(\theta) = r_z'(\theta + \phi) + e_{TX}(\theta) \cdot \sin\phi - e_{TY}(\theta) \cdot \cos\phi, \tag{5.26}$$

$$\nu_3(\theta) = r_z'(\theta + \tau) + e_{TX}(\theta) \cdot \sin\tau - e_{TY}(\theta) \cdot \cos\tau. \tag{5.27}$$

The differential outputs for calculating the $e_{TX}(\theta)$ and $e_{TY}(\theta)$ are expressed by:

$$\begin{aligned}\Delta\nu_{TX}(\theta) &= a_3 \cdot \nu_1(\theta + \phi) - a_3 \cdot \nu_2(\theta) + a_4 \cdot \nu_3(\theta) - a_4 \cdot \nu_1(\theta + \tau) \\ &\quad + a_5 \cdot \nu_2(\theta + \tau) - a_5 \cdot \nu_3(\theta + \phi) \\ &= e_{TX}(\theta) + a_1 \cdot e_{TX}(\theta + \phi) + a_2 \cdot e_{TX}(\theta + \tau),\end{aligned} \tag{5.28}$$

$$\begin{aligned}\Delta\nu_{TY}(\theta) &= a_1 \cdot \nu_2(\theta) - a_1 \cdot \nu_1(\theta + \phi) + a_2 \cdot \nu_3(\theta) - a_2 \cdot \nu_1(\theta + \tau) \\ &= e_{TY}(\theta) + a_1 \cdot e_{TY}(\theta + \phi) + a_2 \cdot e_{TY}(\theta + \tau),\end{aligned} \tag{5.29}$$

where a_1 and a_2 are those defined in Equation 5.20. a_3, a_4 and a_5 are defined by

$$a_3 = \frac{\cos\tau}{\sin(\tau-\phi)},\ a_4 = \frac{\cos\phi}{\sin(\tau-\phi)},\ a_5 = \frac{1}{\sin(\tau-\phi)}. \tag{5.30}$$

Figure 5.8 shows a schematic of the 2D slope sensor unit designed and constructed for experiments. The sensor unit consists of three 2D slope sensors. The angles ϕ and τ between sensors were designed to be 60 and 96º, respectively. This sensor arrangement makes the three-slope sensor method sensitive to undulations per revolution of up to 28, which is the highest calculation number in the experiments. It should be pointed out that the sensor arrangement is needed to be optimized if it is necessary to measure higher undulations per revolution. The sensors utilize the principle of autocollimation for slope detection. As can be seen from the schematic of sensor 1, a collimated beam from a laser diode is projected onto point *A* on the workpiece surface after passing through a polarization beam splitter (PBS) and a quarter waveplate. The reflected beam is reflected again at the PBS and then accepted by the autocollimation unit consisting of an objective lens and a quadrant photodiode (QPD) placed at the focal position of the lens. The 2D

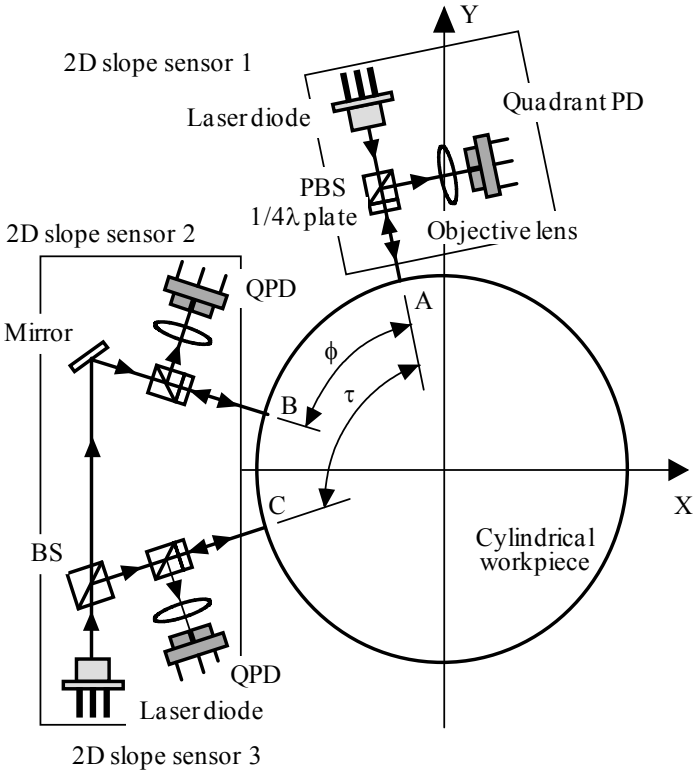

Figure 5.8. Schematic of the two-dimensional slope sensor unit for the three-slope sensor method

slope information at point *A* can be obtained from the photoelectric currents of the QPD. Sensors 2 and 3 share the same optical source for the purpose of compactness. The laser beam is divided into two beams by a beam splitter (BS). The beams are projected onto points *B* and *C* on the workpiece surface. The reflected beams are received by two autocollimation units so that the 2D slope information at points *B* and *C* can be detected, respectively. Diameters of the laser beams were set to be 0.5 mm and focal distances of the lenses were 30 mm. The slope sensitivity of the sensors was approximately 0.1 arcsec. The size of sensor A was 90 mm (*L*) × 80 mm (*W*) × 40 mm (*H*) and that of sensors B and C was 160 mm (*L*) × 100 mm (*W*) × 40 mm (*H*).

Figure 5.9 shows a schematic of the experimental setup for roundness and spindle error measurement. A diamond turned cylindrical workpiece with a diameter of 80 mm was employed as the artifact. The workpiece was mounted on an air-spindle. The outputs of the slope sensors were sampled simultaneously by a personal computer via a 12-bit AD converter. The rotational angle of the spindle was measured by an optical encoder. The roundness of the workpiece was also measured by the conventional three-displacement sensor method employing three capacitive-type displacement sensors for comparison. The measured spindle error and workpiece roundness are shown in Figures 5.10 and 5.11, respectively.

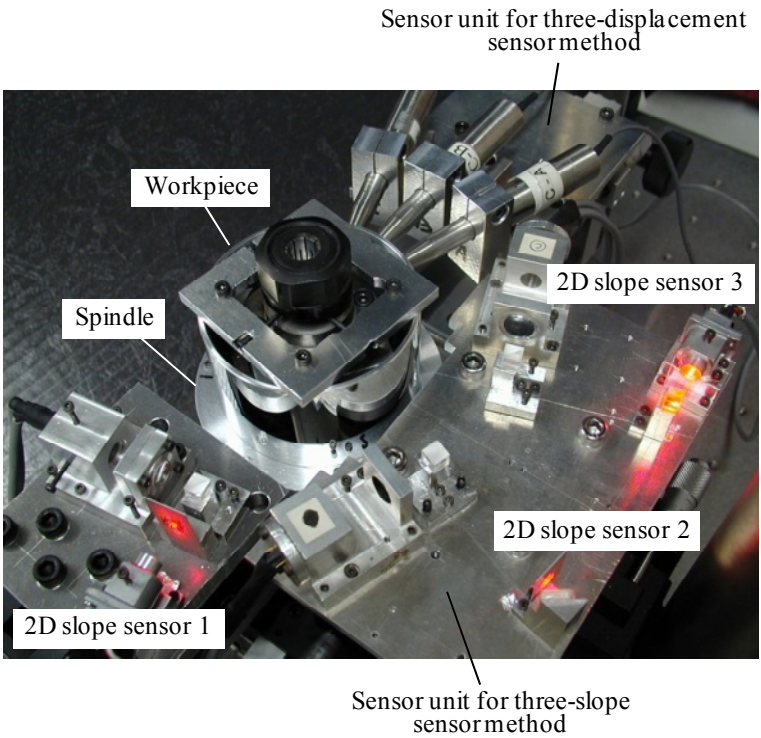

Figure 5.9. Photograph of the experimental setup for roundness and spindle error measurement by the three-slope sensor method

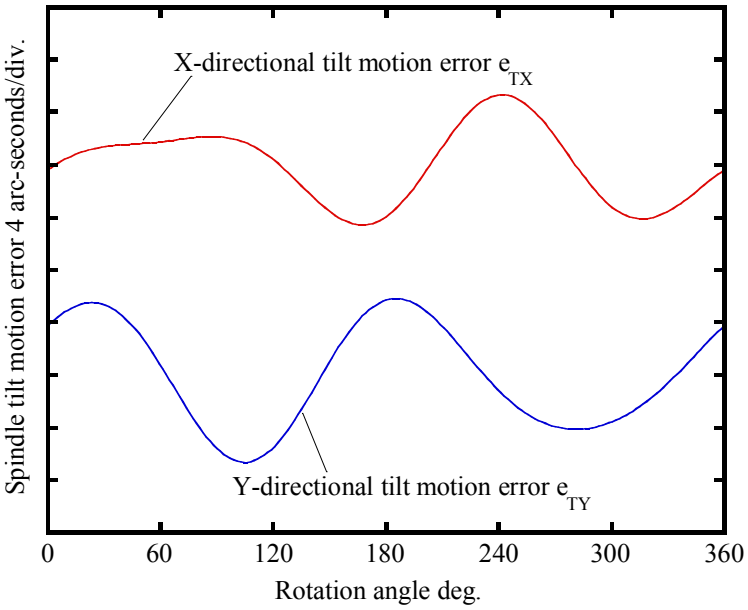

(a) Tilt motion error

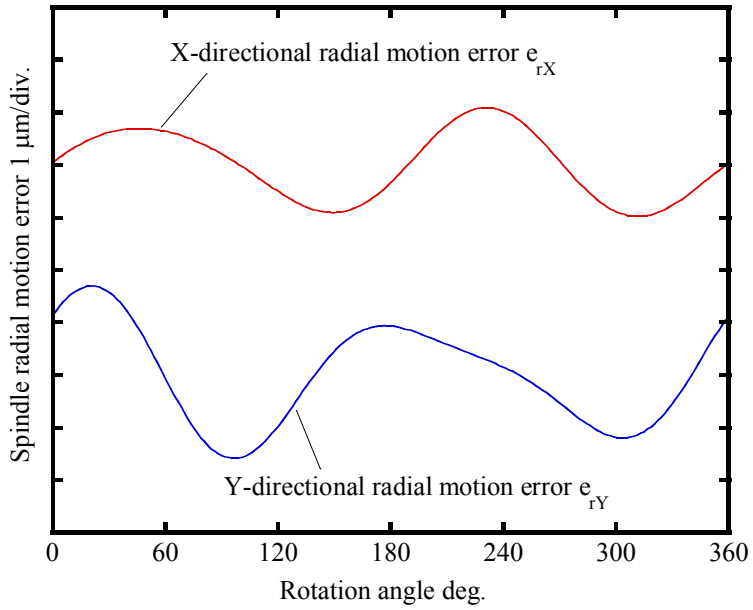

(b) Radial motion error

Figure 5.10. Measured spindle motion error

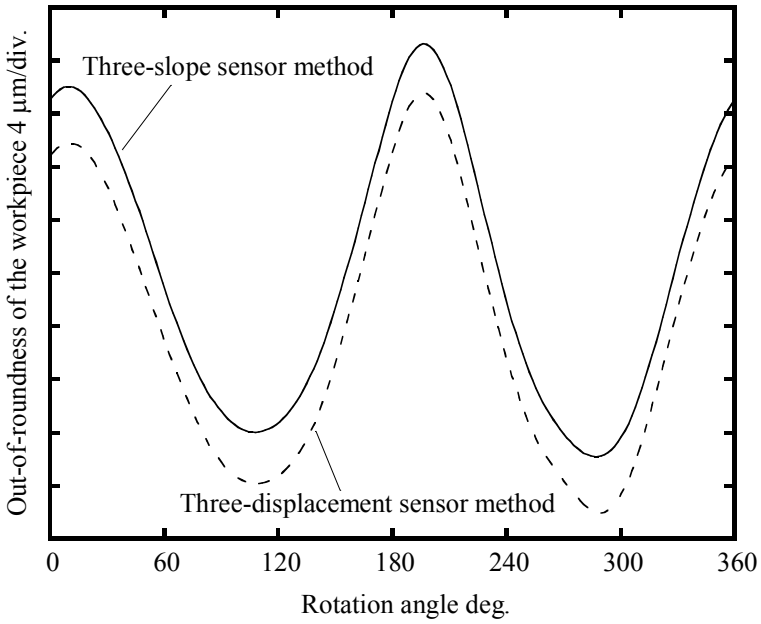

(a) Rectilinear plot

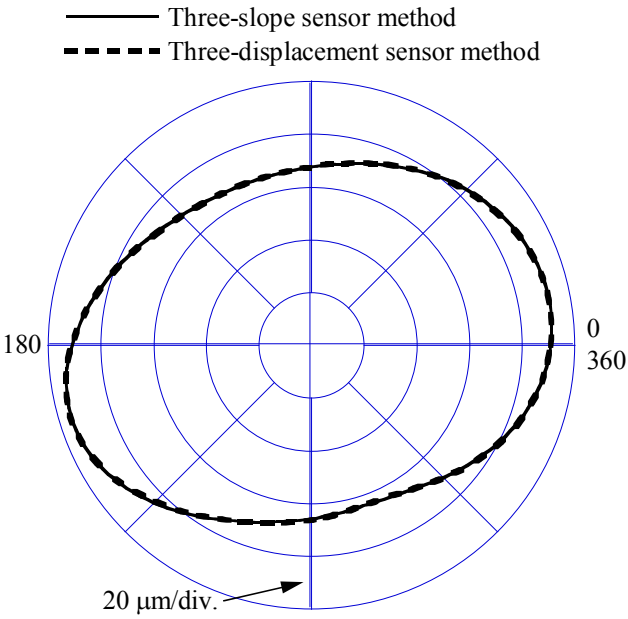

(b) Polar plot

Figure 5.11. Measured workpiece roundness

In the experiment, the spindle speed was approximately 60 rpm and the sampling number over one revolution was 200. Figure 5.10 (a) shows the two-directional components of the tilt error motion, which were approximately 9.9 arcsec in the *X*-direction and 12.0 arcsec in the *Y*-direction, respectively. The two-directional components of the radial error motion of the spindle are plotted in Figure 5.10 (b). The *X*-directional component was approximately 2.0 μm and the *Y*-directional component was approximately 3.3 μm. Figure 5.11 shows the measured roundness of the cylindrical workpiece. The roundness was approximately 31.1 μm. The same workpiece was also measured by the conventional three-displacement sensor method and the result was shown in the figure. It can be seen that the two results corresponded well with each other.

5.3 Mixed Method

The three-sensor method described above can separate the workpiece roundness error from the spindle error motion. However, some frequency components of roundness cannot be accurately measured using this method because of the problem of harmonic suppression. This problem cannot be completely solved by merely increasing the number of sensors [11, 14]. In this section, a method of mixing the displacement sensors and the slope sensors, which is called the mixed method, is described. This method can separate the roundness error from the spindle error completely, and capture high-frequency components.

Figure 5.12 shows the schematics of the two-displacement/one-slope (2D1S) mixed method and the one-displacement/two-slope (1D2S) mixed method. In the 2D1S mixed method, two displacement sensors (sensors 1 and 3) and one slope sensor (sensor 2) are employed. Let ϕ and τ be the angles between the sensors. The sensor outputs in the 2D1S mixed method are expressed by:

$$m_1(\theta) = r(\theta) + e_Y(\theta), \tag{5.31}$$

$$\mu_2(\theta) = r'(\theta + \phi) + \frac{e_X(\theta)}{R_r}\cos\phi - \frac{e_Y(\theta)}{R_r}\sin\phi, \tag{5.32}$$

$$m_3(\theta) = r(\theta + \tau) + e_X(\theta)\sin\tau + e_Y(\theta)\cos\tau. \tag{5.33}$$

The differential output $m_{2D1S}(\theta)$ to cancel the spindle error can be denoted as:

$$\begin{aligned} m_{2D1S}(\theta) &= m_1(\theta)(\tan\phi + \cot\tau) - \frac{m_3(\theta)}{\sin\tau} + \frac{R_r\mu_2(\theta)}{\cos\phi} \\ &= r(\theta)(\tan\phi + \cot\tau) - \frac{r(\theta+\tau)}{\sin\tau} + \frac{R_r r'(\theta+\phi)}{\cos\phi}. \end{aligned} \tag{5.34}$$

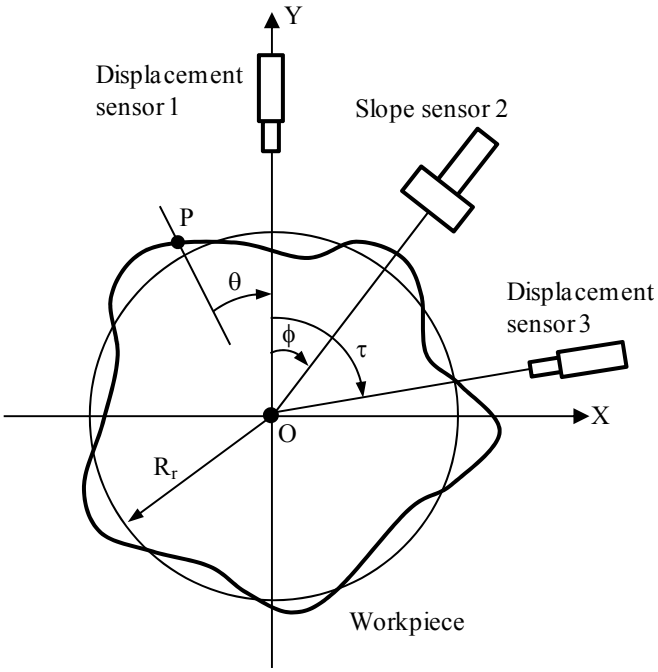

(a) The two-displacement/one-slope (2D1S) mixed method

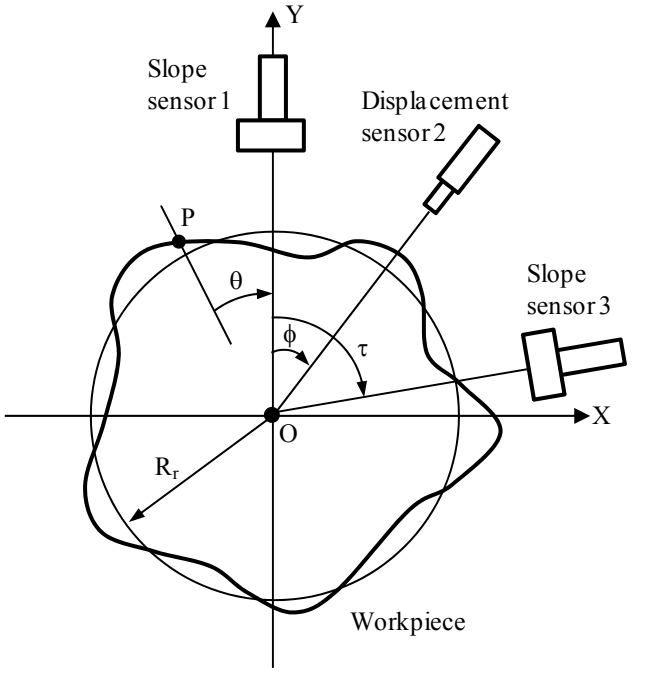

(b) The one-displacement/two-slope (1D2S) mixed method

Figure 5.12. The mixed method mixing displacement probes and slope probes for roundness measurement

Let the Fourier transforms of $r(\theta)$ and $m_{2D1S}(\theta)$ be $R(n)$ and $M_{2D1S}(n)$, respectively, the transfer function of the 2D1S mixed method can be defined by:

$$H_{2D1S}(n) = \frac{M_{2D1S}(n)}{R(n)} = \tan\phi + \cot\tau - \frac{e^{jn\tau}}{\sin\tau} + \frac{jne^{jn\phi}}{\cos\phi}, \tag{5.35}$$

where n is the frequency. The amplitude (harmonic sensitivity) and the phase angle of $H_{2D1S}(n)$ are expressed as:

$$\left|H_{2D1S}(n)\right| = \frac{1}{\cos\phi\sin\tau}[(\sin\phi\sin\tau + \cos\phi\cos\tau - \cos\phi\cos n\tau - n\sin n\phi\sin\tau)^2 + (n\cos n\phi\sin\tau - \cos\phi\sin n\tau)^2]^{1/2}, \tag{5.36}$$

$$\arg[H_{2D1S}(n)] = \tan^{-1}[(n\cos n\phi\sin\tau - \cos\phi\sin n\tau)/(\sin\phi\sin\tau + \cos\phi\cos\tau - \cos\phi\cos n\tau - n\sin n\phi\sin\tau)]. \tag{5.37}$$

We can also employ one displacement sensor and two slope sensors to construct the mixed method as shown in Figure 5.12 (b). The sensor outputs of the 1D2S mixed method can be expressed as:

$$\mu_1(\theta) = r'(\theta) + \frac{e_X(\theta)}{R_r}, \tag{5.38}$$

$$m_2(\theta) = r(\theta+\phi) + e_X(\theta)\sin\phi + e_Y(\theta)\cos\phi, \tag{5.39}$$

$$\mu_3(\theta) = r'(\theta+\tau) + \frac{e_X(\theta)}{R_r}\cos\tau - \frac{e_Y(\theta)}{R_r}\sin\tau. \tag{5.40}$$

The differential output, in which the effect of the spindle error is cancelled, can be given by:

$$m_{1D2S}(\theta) = R_r\mu_1(\theta)(\tan\phi + \cot\tau) - \frac{m_2(\theta)}{\cos\phi} - \frac{R_r\mu_3(\theta)}{\sin\tau}. \tag{5.41}$$

The transfer function of the 1D2S mixed method can be defined as follows:

$$H_{1D2S}(n) = \frac{M_{1D2S}(n)}{R(n)} = jn(\tan\phi + \cot\tau) - \frac{e^{jn\phi}}{\cos\phi} - \frac{jne^{jn\tau}}{\sin\tau}, \tag{5.42}$$

$$|H_{1D2S}(n)| = \frac{1}{\cos\phi \sin\tau}[(n\cos\phi\sin n\tau - \cos n\phi \sin\tau)^2$$

$$+(n\sin\phi\sin\tau + n\cos\phi\cos\tau - \sin n\phi\sin\tau$$

$$-n\cos\phi\cos n\tau)^2]^{1/2}, \tag{5.43}$$

$$\arg[H_{1D2S}(n)] = \tan^{-1}[(n\sin\phi\sin\tau + n\cos\phi\cos\tau - \sin n\phi\sin\tau$$

$$-n\cos\phi\cos n\tau)/(n\cos\phi\sin\tau - \cos n\phi\sin\tau)], \tag{5.44}$$

where $M_{1D2S}(n)$ is the Fourier transform of $m_{1D2S}(\theta)$.

With the angular distances ϕ and τ acting as parameters, the amplitudes of the transfer functions (harmonic sensitivities) of the two methods are plotted in Figure 5.13, respectively. As can be seen in the figures, there is no frequency at which the harmonic sensitivity approaches zero, indicating that both the two mixed methods can measure high-frequency components correctly. In comparison with the 2D1S mixed method, the 1D2S mixed method is more sensitive when $n \leq 7$. On the other hand, the 2D1S mixed method is superior to the 1D2S mixed method in the higher-frequency range. The harmonic sensitivity of the 2D1S mixed method in the low-frequency range, and that of 1D2S mixed method in the high-frequency range can be seen to be closely related to the sensor arrangement. As shown in Figure 5.13 (a), the minimum harmonic sensitivity $|H_{2D1S}(2)|$ is only 0.16 for the symmetrical sensor arrangement (ϕ, τ) = (22.5º, 45º). This value can be increased by changing the sensor arrangement to one that is asymmetrical. For a fixed τ, the largest $|H_{2D1S}(2)|$ is obtained when ϕ is equal to 0º or τ. In this sensor arrangement, the slope sensor and one of the displacement sensors are placed at the same position. $|H_{2D1S}(2)|$ also improves as β increases. When (ϕ, τ) = (0º, 90º) or (ϕ, τ) = (90º, 90º), $|H_{2D1S}(2)|$ reaches its limiting value. In this sensor arrangement, the 2D1S mixed method yields the most well-balanced harmonic response. The same can be said with regard to the 1D2S mixed method. The mixed method with this sensor arrangement is called the orthogonal mixed method.

Figure 5.14 shows the principle of the orthogonal mixed method. The output $m_1(\theta)$ of the displacement sensor and the output $\mu_2(\theta)$ of the slope sensor can be expressed as follows:

$$m_1(\theta) = r(\theta) + e_Y(\theta), \tag{5.45}$$

$$\mu_2(\theta) = r'(\theta + \frac{\pi}{2}) - \frac{e_Y(\theta)}{R_r}. \tag{5.46}$$

Therefore, the differential output $m_{om}(\theta)$, in which the roundness error is separated from the spindle error, can be denoted as:

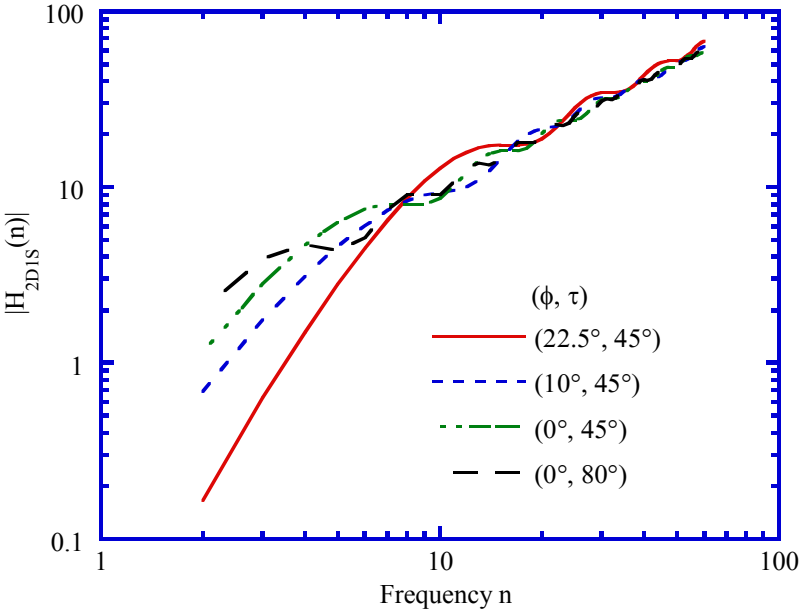

(a) The 2D1S mixed method

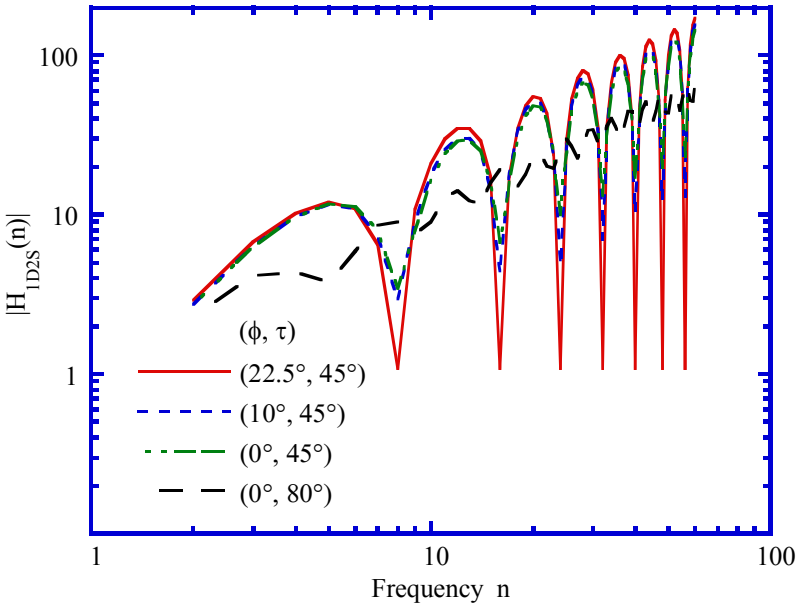

(b) The 1D2S mixed method

Figure 5.13. The harmonic sensitivities of the mixed method

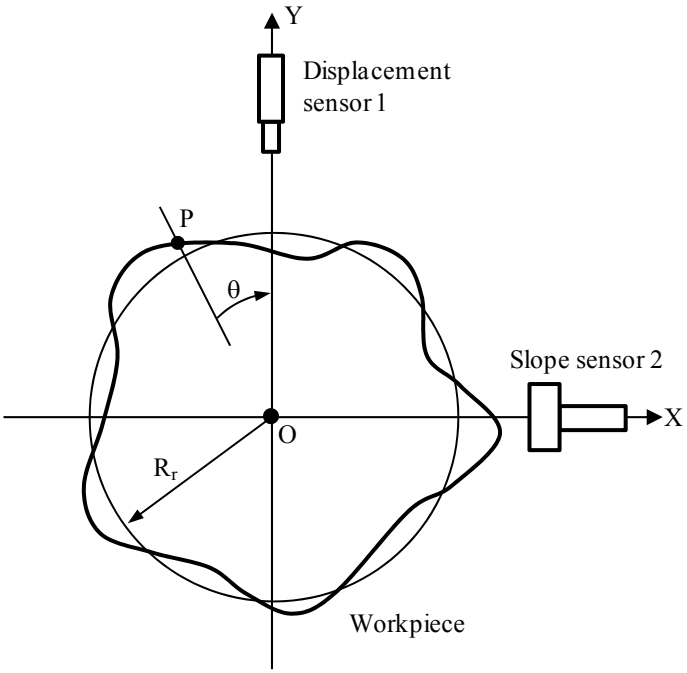

Figure 5.14. The orthogonal mixed method for roundness measurement

$$m_{om}(\theta) = m_1(\theta) + R_r \mu_2(\theta) = r(\theta) + R_r r'(\theta + \frac{\pi}{2}) . \tag{5.47}$$

The transfer function of the orthogonal mixed method can be expressed by:

$$H_{om}(n) = \frac{M_{om}(n)}{R(n)} = 1 + jne^{jn\frac{\pi}{2}} , \tag{5.48}$$

$$\left|H_{om}(n)\right| = [(1 - n\sin n\frac{\pi}{2})^2 + (n\cos n\frac{\pi}{2})^2]^{1/2} , \tag{5.49}$$

$$\arg[H_{om}(n)] = \tan^{-1}[(n\cos n\frac{\pi}{2})/(1 - n\sin n\frac{\pi}{2})] . \tag{5.50}$$

where $M_{om}(n)$ is the Fourier transform of $m_{om}(\theta)$.

Figure 5.15 shows the amplitude of the transfer function (harmonic sensitivity) of the orthogonal mixed method. As can be seen from the figure, $H_{om}(n)$ yields good characteristics. The minimum harmonic sensitivity $|H_{om}(2)|$ is 2.24.

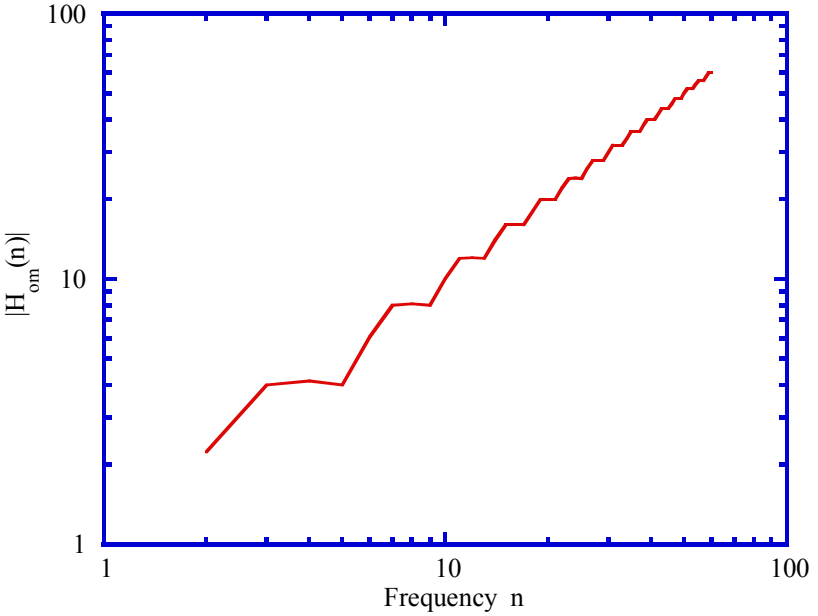

Figure 5.15. The harmonic sensitivity of the orthogonal mixed method

As shown in Figure 5.16, if a setting error $\Delta\phi$ in the angular distance between the two sensors exists, the differential output of the orthogonal mixed method becomes

$$m_e(\theta) = r(\theta + \Delta\phi) + R_r r(\theta + \frac{\pi}{2})$$

$$\approx r(\theta) + R_r r'(\theta + \frac{\pi}{2}) + \Delta\phi r'(\theta)\,. \tag{5.51}$$

An error $\Delta m_{om}(\theta)$ in the differential output occurs as:

$$\Delta m_{om}(\theta) = \Delta\phi r'(\theta)\,. \tag{5.52}$$

The evaluated Fourier transform $R_e(n)$ of the roundness error then becomes

$$R_e(n) = \frac{M_e(n)}{H_{om}(n)}$$

$$= R(n) + \frac{\Delta M_e(n)}{H_{om}(n)}$$

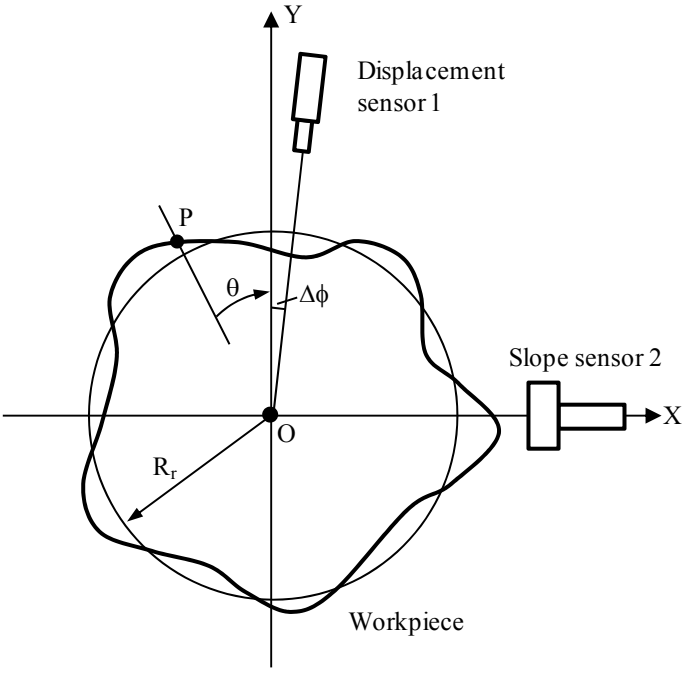

Figure 5.16. Setting error of angular distance

$$= R(n) + \Delta R(n), \tag{5.53}$$

where

$$R_e(n) = \frac{\Delta M_e(n)}{H_{om}(n)}. \tag{5.54}$$

Here, $R(n)$ is the real Fourier transform of the roundness error. $M_e(n)$ and $\Delta M_e(n)$ are the Fourier transforms of $m_e(\theta)$ and $\Delta m_e(\theta)$, respectively. The relative error of $|R_e(n)|$ to $|R(n)|$ can then be evaluated as:

$$\Delta E(n) = 1 - \left|\frac{R_r(n)}{R(n)}\right| = \left|\frac{\Delta R_r(n)}{R(n)}\right|$$

$$= \frac{n\Delta\phi}{\left|H_{om}(n)\right|}. \tag{5.55}$$

Figure 5.17 shows $\Delta E(n)$ plotted versus n when $\Delta\phi = 0.5^{\circ}$. It can be seen that the largest error occurs at $n = 5$ ($\Delta E(5) = 1.1\%$).

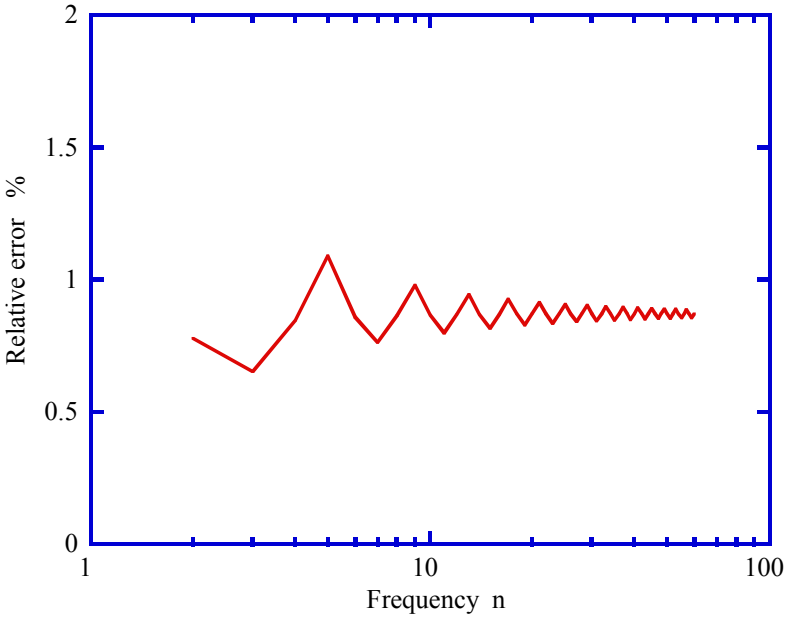

Figure 5.17. Evaluation error of roundness caused by the setting error

An optical sensor system consisting of one displacement sensor [17] and one slope sensor [18] with an angular distance of 90º was constructed to realize the orthogonal mixed method. Both the displacement sensor and the slope sensor utilize the principle of the critical angle method of total reflection.

Figure 5.18 shows the experimental setup for displacement sensor calibration. A capacitive sensor was used as the reference. The surface was moved by using a PZT actuator, and the displacement of the surface was simultaneously measured by the developed displacement sensor and the reference sensor. Figure 5.19 shows calibration results obtained in two separate measurements. The residual error from fitting with a third-order polynomial is also plotted in this figure, and can be seen to be approximately 0.5% of the calibration range. Figure 5.20 shows the experimental setup for the slope sensor calibration. A photoelectric autocollimator was used as the reference. A lever system was used to introduce the angular displacement. The lever was driven by using a PZT actuator so that the lever could rotate about its fulcrum. The angular displacement of the lever was measured simultaneously by the developed slope sensor and the autocollimator. Two separate calibration results are plotted in Figure 5.21. The residual error from fitting with a third-order polynomial is approximately 0.5% of the calibration range.

The experimental setup shown in Figure 5.22 was used to investigate the feasibility of canceling the spindle error in the differential output of the orthogonal mixed method defined in Equation 5.47. A precision ball with a diameter of 1 inch was used as the target. The spindle error $e_Y(\theta)$ was introduced by moving the ball in the Y-direction by using a PZT. As shown in Figure 5.23, the spindle error $e_Y(\theta)$ is canceled in the differential output of the orthogonal mixed method.

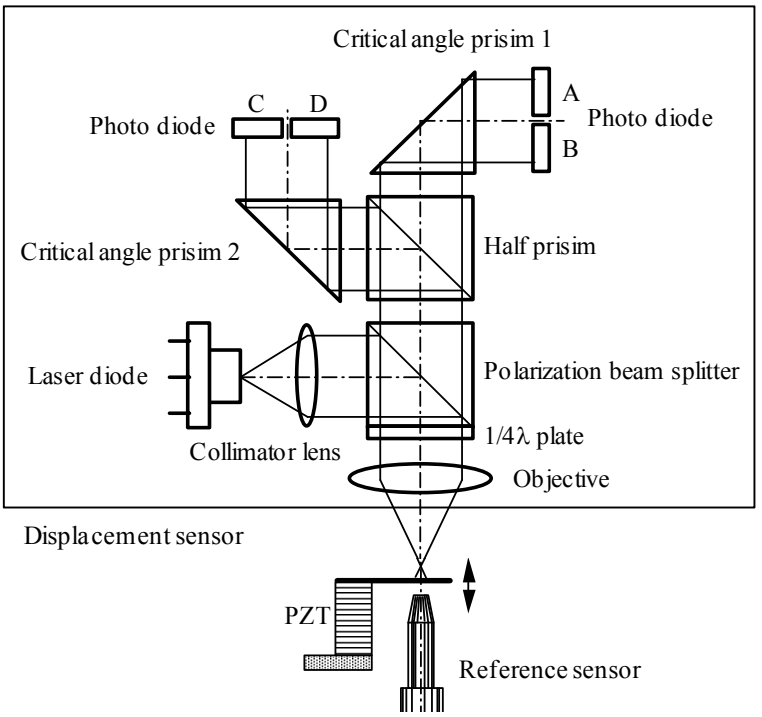

Figure 5.18. Setup for calibration of the displacement probe

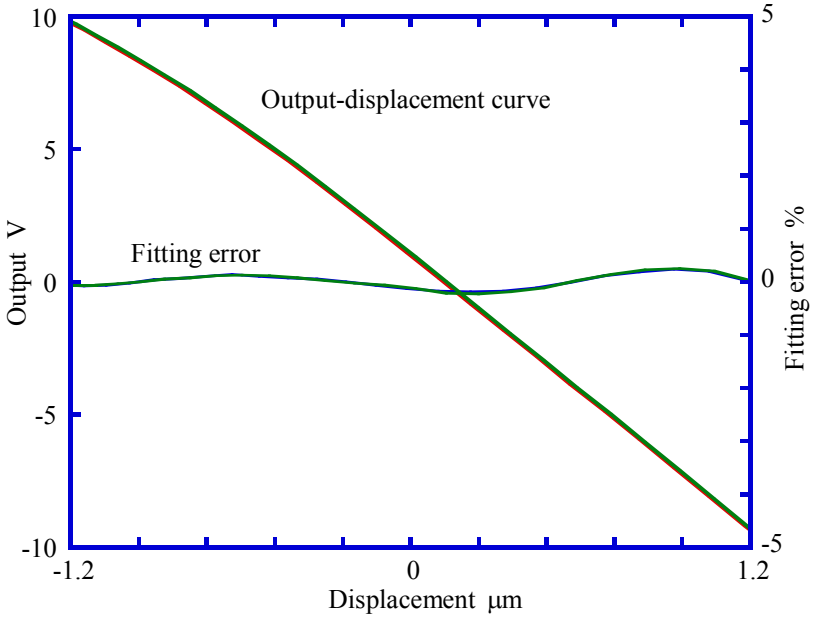

Figure 5.19. Calibration of the displacement sensor

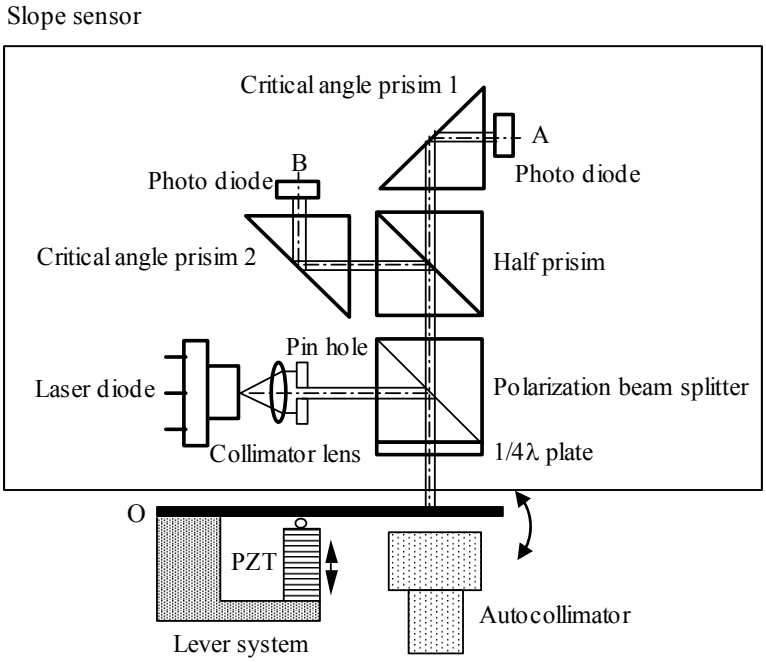

Figure 5.20. Setup for calibration of the slope probe

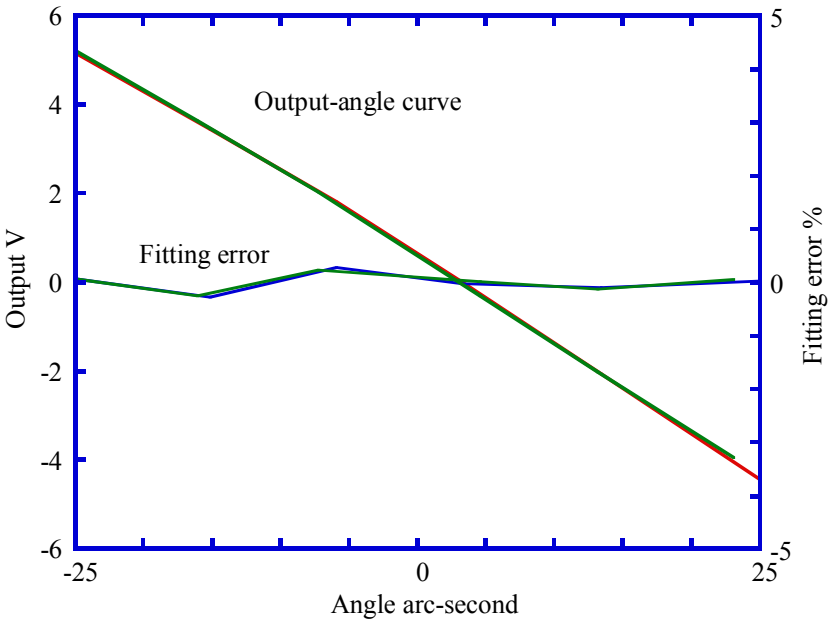

Figure 5.21. Calibration result of the slope probe

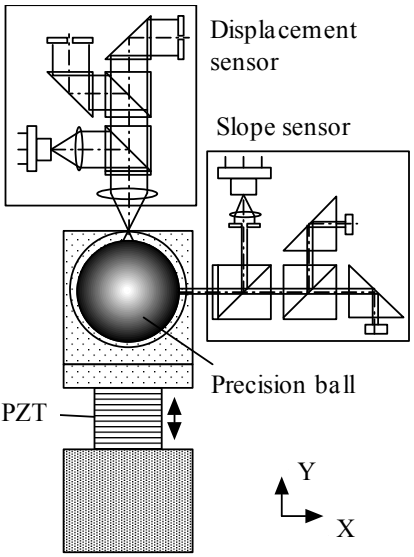

Figure 5.22. Setup for testing of the differential output of the orthogonal mixed method

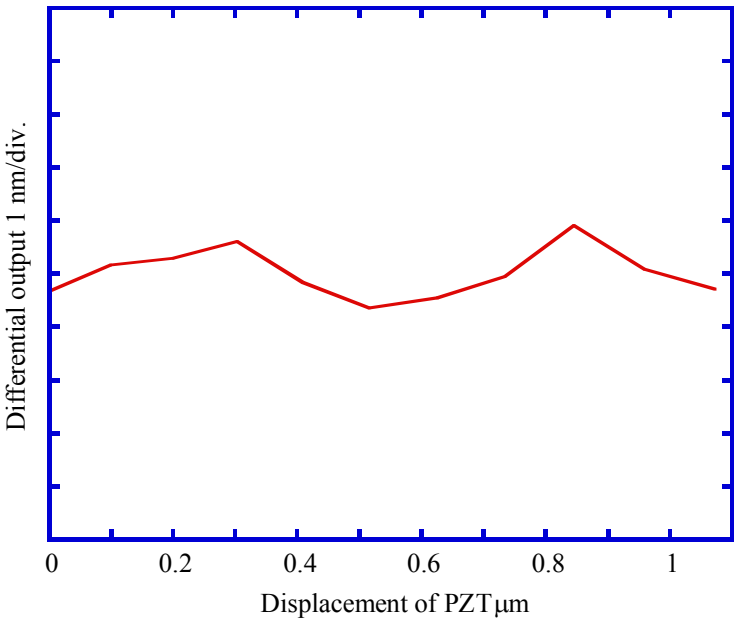

Figure 5.23. Differential output of the orthogonal mixed method

Figure 5.24 shows a photograph of the experimental measurement system constructed for the roundness measurement based on the orthogonal mixed method. The measurement system consists of the developed displacement and slope sensors, the precision ball shown in Figure 5.22, an air-spindle, and an optical rotary encoder. The rotational angle of the spindle was measured by the optical encoder. The positional signal of the optical encoder is sent to the AD converter as a trigger signal. The output signals are sampled simultaneously in order to avoid errors attributable to the sampling time delay. The ball can be adjusted in the *X*- and *Y*-directions by using adjustment screws so that the eccentric error can be adjusted to fall within the measurement ranges of the sensors. The sensors are mounted on *XYZ* micro-stages and the positions of the sensors relative to the ball can be adjusted in the *X*-, *Y*- and *Z*-directions.

Figure 5.25 shows the result of stability test of the optical sensor. In the test, the output signals were sampled without rotating the ball. The displacement sensor and the slope sensor can be seen to have the stabilities of 1 nm and 0.01 arc-second, respectively in a test term of 20 s.

Figure 5.26 shows the measured roundness errors of two separate measurements and the repeatability error between the two measured results. Figure 5.26 (a) shows the polar plot of the roundness error and the repeatability error, and Figure 5.26 (b) shows the corresponding rectilinear plot. The sampling number was 512. It can be seen that the roundness error is approximately 60 nm, and the repeatability error is approximately 5 nm. The measured spindle errors of the two repeated measurements and the difference between them are shown in Figure 5.27. The spindle error was approximately 800 nm, and the difference was approximately 140 nm. Vibration components, which were caused by the improper coupling between the spindle and the encoder, were found in the spindle errors. Comparison of the results plotted in Figures 5.26 and 5.27 shows that the roundness error is separated from large spindle errors with high repeatability. This confirmed the effectiveness of the orthogonal mixed method.

5.4 Summary

A multi-sensor method using three two-dimensional slope sensors for roundness and spindle error measurement, called the three-slope sensor method, has been described. This method can simultaneously measure the workpiece roundness error, the spindle radial error motion and the spindle tilt error motion accurately.

A multi-sensor method mixing displacement sensors and slope sensors for roundness and spindle error measurement, known as the mixed method, has also been presented. This method can separate roundness and spindle error completely, and is well suited for measuring profiles that include high-frequency components. It was verified that well-balanced harmonic response can be achieved over the entire frequency range when the angular distance between the slope sensor and the displacement sensor is set to be 90º. The mixed method employing this sensor arrangement is called the orthogonal mixed method. This sensor arrangement is also the simplest one because the separation of the roundness error from the spindle error requires only one displacement sensor and one slope sensor.

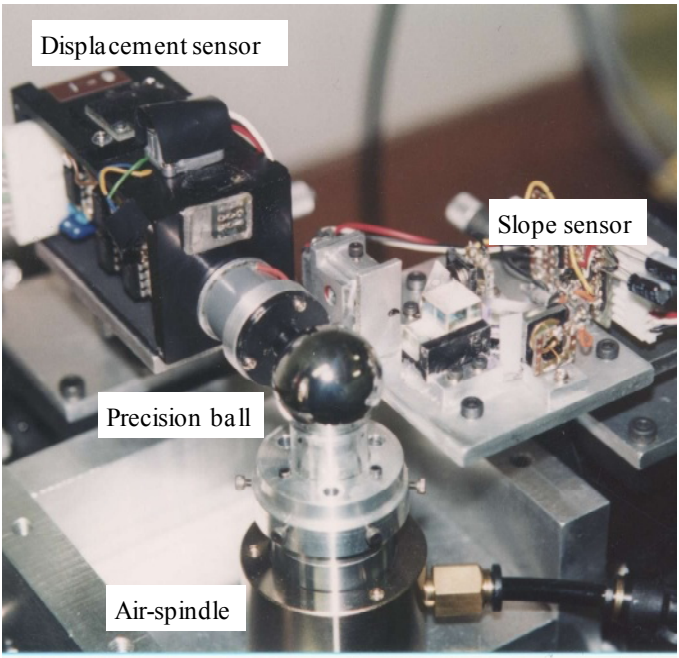

Figure 5.24. Setup for roundness and spindle error measurement with the orthogonal mixed method

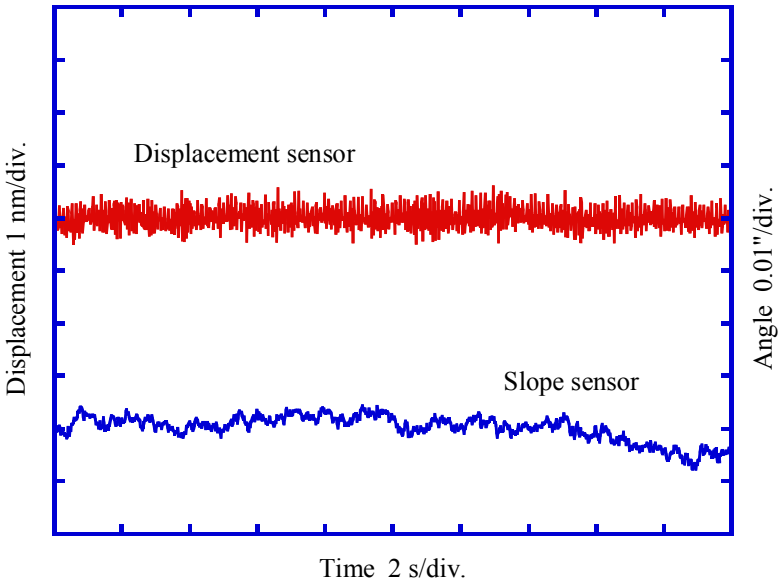

Figure 5.25. Results of stability test

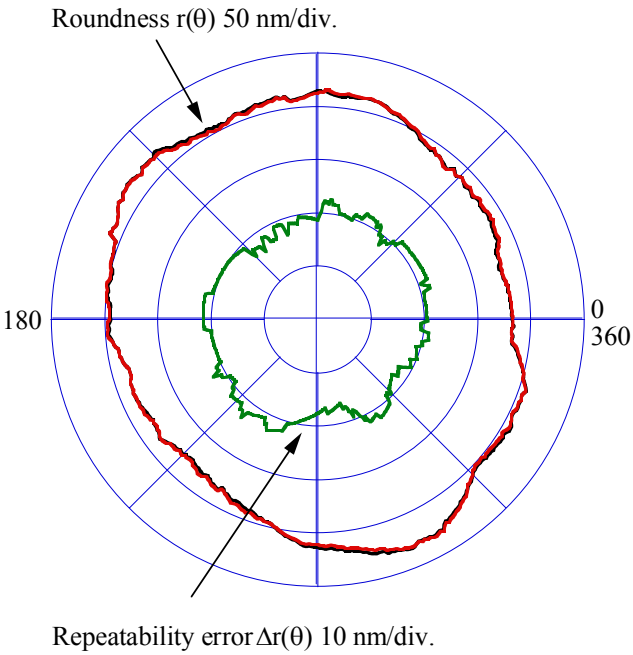

(a) Polar plot

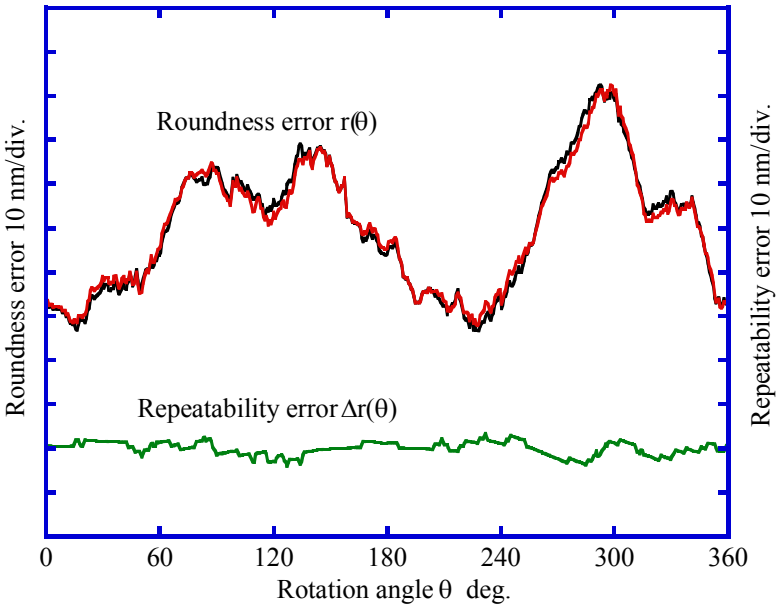

(b) Rectilinear plot

Figure 5.26. Measurement result of ball roundness

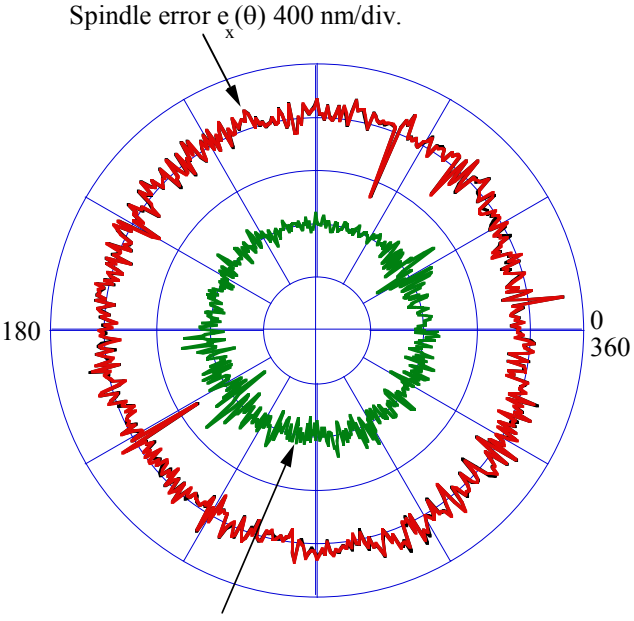

(a) Polar plot

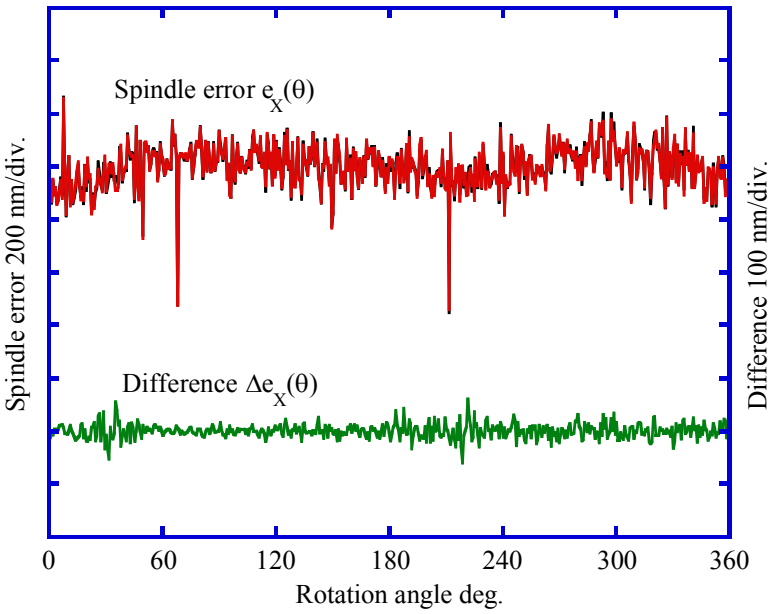

(b) Rectilinear plot

Figure 5.27. Measurement result of spindle error

References

[1] Bryan J, Clouser, R, Holland E (1967) Spindle accuracy. Amer Machinist 612:149–164

[2] CIRP STC Me (1976) Unification document Me: axes of rotation. Ann CIRP 25(2):545–564

[3] Kakino Y, Kitazawa J (1978) In situ measurement of cylindricity. Ann CIRP 27(1):371–375

[4] Shinno H, Mitsui K, Tanaka N, Omino T, Tabata T (1987) A new method for evaluating error motion of ultra-precision spindle. Ann CIRP 36(1):381–384

[5] Whitehouse DJ (1976) Some theoretical aspects of error separation techniques in surface metrology. J Phys E Sci Instrum 9:531–536

[6] Donaldson RR (1972) A simple method for separating spindle error from test ball roundness error. Ann CIRP 21(1):125–126

[7] Evans CJ, Hocken RJ, Estler WT (1996) Self-calibration: reversal, redundancy, error separation and "absolute testing". Ann CIRP 45(2):617–634

[8] Estler WT, Evans CJ, Shao LZ (1997) Uncertainty estimation for multi-position form error metrology. Precis Eng 21(2/3):72–82

[9] Ozono S (1974) On a new method of roundness measurement based on the three points method. In: Proceedings of the International Conference on Production Engineering, Tokyo, Japan, pp 457–462

[10] Moore D (1989) Design considerations in multi-probe roundness measurement. J Phys E Sci Instrum 9:339–343

[11] Zhang GX, Wang RK (1993) Four-point method of roundness and spindle error measurements. Ann CIRP 42(1):593–596

[12] Gao W, Kiyono S, Nomura T (1996) A new multi-probe method of roundness measurements. Precis Eng 19(1):37–45

[13] Gao W, Kiyono S, Sugawara T (1997) High accuracy roundness measurement by a new error separation method. Precis Eng 21(2/3):123–133

[14] Ozono S, Hamano Y (1976) On a new method of roundness measurement based on the three-point method, 2nd report. Expanding the measurable maximum frequency. In: Proceedings of the Annual Meeting of JSPE, pp 503–504

[15] Hanmming RW (1989) Digital filters. Prentice Hall, Upper Saddle River, NJ

[16] Gao W, Kiyono S, Satoh E (2002) Precision measurement of multi-degree-of-freedom spindle errors using two-dimensional slope sensors. Ann CIRP 52(2):447–450

[17] Kohno T, Ozawa N, Miyamoto K, Musha T (1988) High precision optical surface sensor. Appl Opt 27(1):103–108

[18] Huang P, Kiyono S, Kamada O (1992) Angle measurement based on the internal-reflection effect: a new method. Appl Opt 31(28):6047–6055